Evidence for the Exposure of Water Ice on Titan's Surface

Caitlin A. Griffith,[1]* Tobias Owen,[2] Thomas R. Geballe,[3] John Rayner,[2] Pascal Rannou[4]

The smoggy stratosphere of Saturn's largest moon, Titan, veils its surface from view, except at narrow wavelengths centered at 0.83, 0.94, 1.07, 1.28, 1.58, 2.0, 2.9, and 5.0 micrometers. We derived a spectrum of Titan's surface within these "windows" and detected features characteristic of water ice. Therefore, despite the hundreds of meters of organic liquids and solids hypothesized to exist on Titan's surface, its icy bedrock lies extensively exposed.

Titan's thick haze obscures a surface expected to harbor both the source and sink of much of Titan's atmosphere. Methane, the second most abundant atmospheric constituent (~0.05 bar) detected after N_2 (1.4 bar), is continually and irreversibly destroyed by solar ultraviolet photolysis, a process rapid enough to require a recent supply of methane (*1*). Two end-member scenarios are possible. Ongoing geologic activity supplies atmospheric methane (and leads to an atmosphere that varies in size with supply), or ocean reservoirs of methane exist as a result of past geologic activity (*2*, *3*). The products of methane photolysis, a variety of simple and complex organic compounds, precipitate to Titan's surface, leaving a history of Titan's atmospheric composition. If Titan's atmosphere has existed in its present form since its formation, ~800 m of organic liquids and solids blanket Titan's surface (*1*).

Previous efforts to determine Titan's surface composition focused on relatively small spectral regions. Surface albedos at 1.28, 1.58, and 2.0 μm match the spectra of both water ice (*4*, *5*) and solid organic sediments (*6*, *7*). Surface albedos at 1.07 and 1.28 μm are ~100% higher than that at 1.58 μm, also consistent with water ice and aged tholins (laboratory analogs of Titan's organic haze), although notably not young tholins (*7*). Titan's 5-μm surface albedo (*8*) exceeds that at 3 μm (*9*) but is smaller than 1- to 2-μm values, again consistent with the dirty water ice found on icy Jovian satellites and the haze sediments expected for Titan's surface (*7*).

Here, we analyze Titan's 0.8- to 5.1-μm spectrum to derive surface albedos at the eight window wavelengths. Our study builds on previous work (*4*, *5*, *8*, *9*), because the broad spectral features characteristic of solids (i.e., surface constituents) emerge only with the examination of a large spectral range.

We recorded observations at the United Kingdom Infrared Telescope (UKIRT) with the CGS4 spectrometer (Fig. 1, Table 1) and at NASA's Infrared Telescope Facility (IRTF) with the new SpeX spectrograph (*10*). Two grating positions, overlapping in wavelength coverage, provide correct relative albedos from 0.8 to 5.1 μm (Fig. 1). The data's 2- to 2.3-μm flux ratios agree within 2% with previous data devoid of cloud events (*11*), indicating relatively cloud-free conditions on Titan. Division of Titan's raw spectra by those of the observed G stars (Table 1) eliminates most telluric absorption features. Considering Titan's optical size (*12*), distances to the Earth and the Sun, and the standard's magnitude, we calculated Titan's geometric albedo (its reflection relative to an isotropically scattering reflector). Fluxes agreed well, within 3%, with previous observations at 0.5 to 1.0 μm (*13*–*15*) and among our dataset, but less well with a study of Titan's 1.05 to 2 μm spectrum (*5*).

We derived Titan's surface reflectivity and atmospheric opacity from radiative transfer calculations (*16*) that simulated the absorption and scattering of sunlight from Titan's atmosphere (*17*, *18*) and produced synthetic spectra that are compared with those observed. We first constrained the main opacity source in the windows, Titan's haze, by examining the spectral regions—0.5 to 0.7 (*14*, *15*), 0.79, 0.9, 1.65, 2.2, 3.1, and 4.8 μm—that are exterior to the windows and most sensitive to the haze (*19*). Haze models specifying the particle size, shape, and density with altitude then bridge the windows to these wavelength regions, thus providing haze optical depths at the windows (*20*).

Several constraints on the opacity of Titan's haze guide our derivation of the haze optical depths. Voyager high phase angle observations indicate an optical depth (at 0.5 μm) of 0.1 at 200 km altitude (*21*). In addition, Titan's surface is discernible at 0.63 μm, indicating an upper limit to the 0.63-μm opacity of the haze (*22*, *23*). (Here, gas absorption is negligible.) At 0.79 μm, the haze

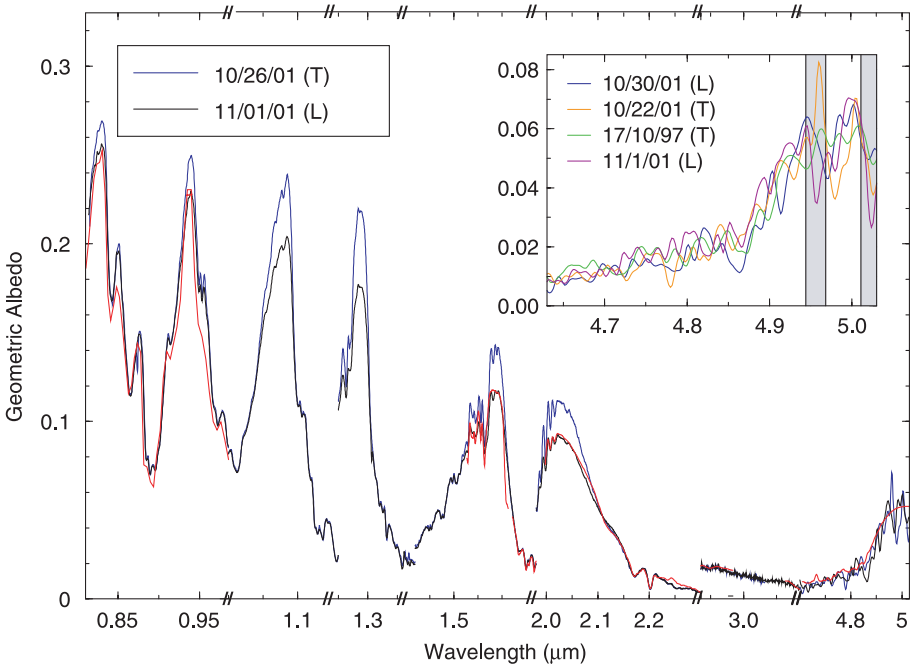

Fig. 1. Titan's leading (blue) and trailing (black) hemispheres (Table 1) display different window albedos, a result of different average surface reflectivities (*22*, *35*–*37*, *48*, *49*). Calculated spectra of the trailing hemisphere appear at wavelengths where methane absorption information exists (red). Within errors, no hemispheric difference appears at the 2.9- and 5-μm windows. (**Inset**) Details of 5-μm spectra of Titan's leading (L) and trailing (T) hemispheres. Fine spectral structure results from smoothed noise coupled with incomplete sky subtraction. Optically thick regions in Earth's atmosphere appear in gray; here, data are unreliable.

[1]Department of Planetary Sciences, University of Arizona, 1629 East University Boulevard, Tucson, AZ 85721–0092, USA. [2]Institute for Astronomy, 2680 Woodlawn Drive, Honolulu, HI 96822, USA. [3]Gemini Observatory, 670 North A'ohoku Place, Hilo, HI 96720, USA. [4]Université Pierre et Marie Curie, 4 Place Jussieu, Paris, France.

*To whom correspondence should be addressed. E-mail: griffith@lpl.arizona.edu

opacity resides essentially above an optically thick (almost black) layer of CH_4, thus allowing for a methane-independent derivation of the haze optical depth. At 1.65, 2.2, 3.1, and 4.8 μm, absorption lines are saturated, rendering Titan's spectrum fairly insensitive to uncertainties in the gas absorption (*4*). The center and wings of CH_4 bands probe altitudes from 70 to 160 km and collectively provide constraints on the haze vertical structure. Our derived haze optical depths (Fig. 2) can be reproduced with models in which Titan's haze is conglomerate in shape, similar to terrestrial smog (*24*–*30*). These values agree with previous models except those that are most optically thin and thick at 0.6 to 0.85 μm (*31*).

Apart from haze, methane and carbon monoxide (at 5 μm) mildly obscure Titan's windows. A carbon monoxide abundance of 20 ± 10 parts per million matches the data within the noise (Fig. 1), consistent with millimeter and near-infrared spectra of Titan (*8*, *32*, *33*). We assumed a methane distribution equivalent to a total column abundance of 3.6-km amagat (*34*). We adopted Karkoshka's (*14*, *15*) absorption coefficients of 0.011 and 0.01 km^{-1} $amagat^{-1}$ at 0.83 μm and 0.94 μm. On the basis of laboratory data of methane (*4*, *9*, *11*), we assumed 0.005 km^{-1} $amagat^{-1}$ at 1.07, 1.28, 1.58, and 2.0 μm (*5*), and 0.07 km^{-1} $amagat^{-1}$ at 2.9 μm. A factor of 2 variations in the methane coefficient changed the surface albedos by 9 to 10% at 0.83 and 0.94, 3 to 4% for the 1- to 2-μm windows, 100% at 2.9 μm, and immeasurably at 5 μm.

With constraints on Titan's atmospheric opacity, we determined the surface reflectivity by reproducing Titan's observed albedo with radiative transfer calculations (Fig. 1). We compared Titan's surface albedos with candidate surface constituents: organic precipitates and water ice (Fig. 2). Organic sediments, such as tholins, strongly absorb at 2.9 μm because of N-H stretching vibration. Equally prominent is its red color or absorption longward of 1.2 μm, as a result of groups containing conjugated C-C and C=C bonds. Water ice absorbs at 2.9 μm because of ν_1 and ν_3 stretch bands, at 1.49 μm because of their first overtone combination, and at 1.9 μm because of the $\nu_2 + \nu_3$ combination band. Shortward of 1 μm, the dirty water ice characteristic of satellites displays a highly reflective and gray spectrum. Neither Titan's leading nor trailing spectra are red, characteristic of complex organic material. Instead, the major absorption bands of water ice are reproduced at 1.49, 2.0, and 2.9 μm. Indeed, Titan's spectra resemble Ganymede's spectrum, dominated by ice features (Fig. 2).

Our observations represent the disk-averaged light from Titan's hemispheres. Images indicate that roughly one-third of Titan's leading hemisphere is more reflective at all 0.8- to 2.0-μm windows than most of the rest of Titan's surface (*22*, *35*–*37*). If this terrain accounts for the leading and trailing albedo differences, it is substantially more reflective than its surroundings in the 0.8- to 1.3-μm windows and somewhat brighter at 1.6 and 2.0 μm, suggesting a purer and/or smaller grain-size ice surface than that of the darker terrain.

The dark component of Titan's surface is poorly constrained. Liquids (e.g., methane and the anticipated precipitates, ethane and propane) darken Titan's terrain (*38*). In addition, a thin dusting of haze over ice lowers Titan's albedo at short wavelengths while leaving its 2.9 and 5.0 reflectivities unaffected, similar to the observed differences between the hemispheres. Both of these terrains are expected. Once the particulates, wafting in the wind or flowing in streams, haphazardly end up in lakes or oceans, they remain coupled to the liquid (*4*). Eventually, the haze particles, heavier than the primary liquids, settle to the bottoms of lakes. The high and dry terrain loses sediments, and lowlands accrue a buffet of organic material.

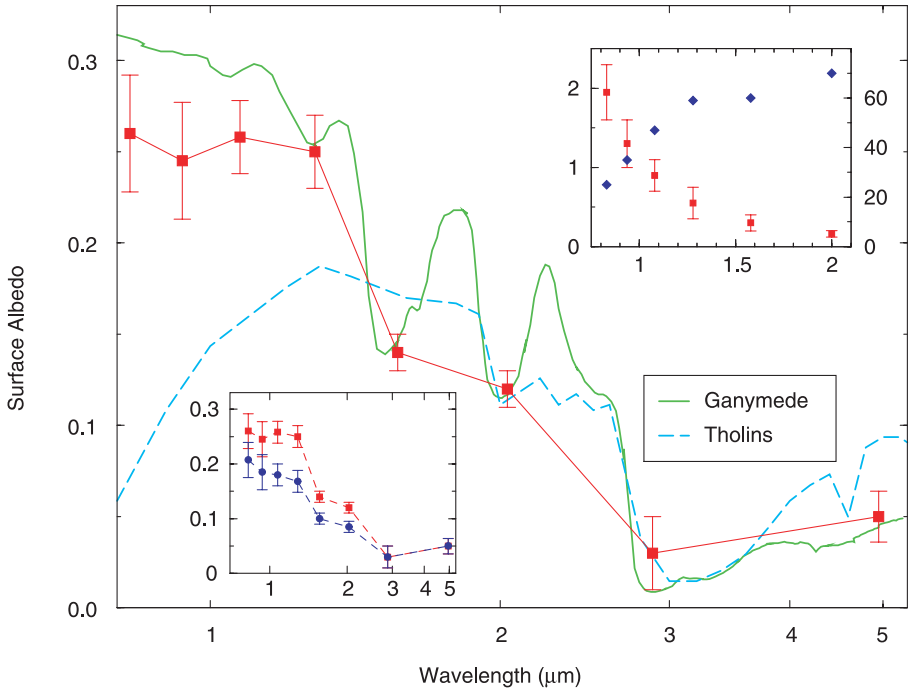

Fig. 2. Titan's leading hemisphere albedo (red squares) resembles that of Ganymede's leading hemisphere (green) (*50*, *51*). The blue dashed line shows a laboratory synthesis of Titan's organic sediment [tholin 4 of Cruikshank *et al.* (*41*)] of 100-μm grain size. Tholin of smaller grain size likely exhibits less pronounced absorption features. The widths of the red squares (half this width shortward of 1.4 μm) represent the wavelength widths of the windows. Errors in Titan's surface albedo are derived assuming 50% uncertainties in the particle sizes and CH_4 optical depth, variations in the haze vertical density consistent with observations, and, at 5 μm, noise. (**Bottom inset**) Surface albedos for Titan's leading (red squares) and trailing (blue circles) hemispheres. (**Top inset**) Haze optical depths (left axis, squares) at window wavelengths, except 2.9 and 5 μm, which have values of 0.3 ± 0.15 and 0.07 ± 0.01, respectively. The disk-averaged percentage of light reflected from Titan's surface (right axis, blue diamonds) reveals that one observes primarily diffuse light, rather than direct light, from Titan's surface at wavelengths below 1.5 μm.

Table 1. Titan spectra. Shown are the wavelengths (micrometers), UT dates of observations, longitude of the sub-Earth point (i.e., the center of the disk), air mass [i.e., 1/cos(θ), where θ is the Titan-to-Earth zenith angle], and the standard stars.

Wavelength	Date	Longitude	Air mass	Standard
4.6–5.2	10/26/97* 10:30	124	1.1-1.9	BS582/G0V
4.6–5.2	10/17/97* 10:00	280	1.04-1.5	BS72/G0V
2.3–5.1	10/22/00† 13:00	260	1.00-1.08	SAO93936/G2V
0.8–5.1	10/26/01† 13:15	293	1.00-1.09	SAO76817/G0
0.8–5.1	10/27/01† 12:30	315	1.00-1.09	SAO76817/G0
0.8–5.1	10/30/01† 12:30	23	1.00-1.10	SAO76817/G0

*Unpublished UKIRT spectra of resolving power R = 500. †New IRTF spectra of resolving power R = 400.

References and Notes

1. Y. L. Yung, M. Allen, J. P. Pinto, *Astrophys. J. Suppl.* **55**, 465 (1984).
2. F. M. Flasar, *Science* **221**, 55 (1983).

3. J. I. Lunine, D. J. Stevenson, Y. L. Yung, *Science* **222**, 1229 (1983).
4. C. A. Griffith, T. Owen, R. Wagener, *Icarus* **93**, 362 (1991).
5. A. Coustenis, E. Lellouch, J. P. Maillard, C. P. McKay, *Icarus* **118**, 87 (1995). Note that their weak CH_4 absorption in the 1 to 2 μm windows (least well constrained) is estimated to be 8 to 18 times greater than our values. Their absolute albedos are ~25 to 50% higher than ours.
6. Haze optical constants come from Khare *et al.* (*39*).
7. Spectra of decade-old tholins (*40*) differ, at 1.2 to 1.4 μm, from spectra of young tholins (*41*). It is not clear whether the tholin chemistry proceeded in isolation or through contamination.
8. Noll *et al.* (*42*) do not consider scattering and emission, causing slightly different results from ours at 5 μm.
9. C. A. Griffith, T. Owen, G. A Miller, T. R. Geballe, *Nature* **395**, 575 (1998). Note that their 1.3 μm surface albedo is incorrect because of faulty normalization of previous observations.
10. J. T. Rayner *et al.*, *Publ. Astron. Soc. Pac.* **115**, 362 (2003).
11. C. A. Griffith, J. L. Hall, T. R. Geballe, *Science* **290**, 509 (2000).
12. O. B. Toon, C. P. McKay, C. A. Griffith, R. P. Turco, *Icarus* **95**, 24 (1992).
13. C. P. McKay, J. B. Pollack, R. Courtin, *Icarus* **80**, 23 (1989).
14. E. Karkoschka, *Icarus* **133**, 134 (1998).
15. E. Karkoschka, *Icarus* **111**, 174 (1994).
16. We adopted a discrete ordinates calculation having eight streams, as described by Stamnes *et al.* (*43*).
17. Titan's thermal profile derives from Lellouch *et al.* (*44*) and Yelle *et al.* (*45*).
18. Absorption coefficients of CH_4 and CO derive from the line parameters of Husson *et al.* (*46*).
19. We varied the vertical optical depth at two altitude regions (40 to 100 km and 100 to 160 km) to derive the range of haze optical depths that fit Titan's spectrum. Haze below ~40 km is limited by the visibility of Titan's surface at 0.63 μm.
20. Our surface albedos are thus unaffected by variations in the 0.01 shape parameter (or width) of our log-normal particle distribution, the tholin optical constants (*6*), and details of the haze models.
21. K. Rages, J. B. Pollack, P. H. Smith, *J. Geophys. Res.* **88**, 8721 (1983).
22. P. H. Smith *et al.*, *Icarus* **119**, 336 (1996).
23. J. Richardson, R. D. Lorenz, A. McEwen, in preparation.
24. M. G. Tomasko, P. H. Smith, *Icarus* **51**, 65 (1982).
25. R. A. West *et al.*, *J. Geophys. Res.* **88**, 8699 (1983).
26. R. A. West, P. H. Smith, *Icarus* **90**, 330 (1991).
27. P. Rannou, M. Cabane, R. Botet, E. Chassefière, *J. Geophys. Res.* **102**, 10997 (1997).
28. P. Rannou *et al.*, *Icarus* **118**, 355 (1997).
29. C. P. McKay *et al.*, *Planet. Space Sci.* **49**, 79 (2001).
30. M. G. Tomasko *et al.*, in *Huygens: Science Payload and Mission, Vol. ESA-SP 1177*, A. Wilson, Ed. (European Space Agency Publications Division, Noordwijk, Netherlands, 1997), pp. 109–138.
31. One model that fits our optical depths contains haze above 90-km altitude, where the radius (in micrometers), column abundance (km amagat) and 0.94-μm optical depth are specified by the values (*a*, *b*, *c*) of (6.8, −424, 0), (152.3, −131.7, −34.5), and (104.3, −108.9, −20.2), respectively. These haze parameters, *x*, depend on altitude, *z* (in km), as: $z = a + b \log_{10}(x) + c[\log_{10}(x)]^2$.
32. B. Lutz, C. de Bergh, T. Owen, *Nature* **220**, 1374 (1983).
33. T. Hidayat *et al.*, *Icarus* **133**, 109 (1998).
34. Methane is assumed to be subsaturated at the surface with a humidity of 60%. A constant mixing ratio is adopted above the surface until the level of saturation is reached. Above this level, the atmosphere is saturated up to the tropopause. The mixing ratio is constant at the tropopause value above this point. An amagat is a unit of density equal to 2.69×10^{19} cm^{-3}.
35. M. Combes *et al.*, *Icarus* **129**, 482 (1997).
36. R. Meier, B. A. Smith, T. C. Owen, R. J. Terrile, *Icarus* **145**, 462 (2000).
37. S. G. Gibbard *et al.*, *Icarus* **139**, 189 (1991).
38. Note that 5-m-deep pools of methane absorb 95% of 1.1- to 5-μm sunlight (*47*).
39. B. N. Khare, C. Sagan, E. T. Arakawa, F. Suits, T. A. Callcott, M. W. Williams *Icarus* **60**, 127 (1984).
40. T. L. Roush, J. B. Dalton, Conf. 33, abstract 1532, Lunar Planetary Inst., Houston, TX (2002).
41. D. Cruikshank *et al.*, *Icarus* **94**, 345 (1991).
42. K. S. Noll, T. R. Geballe, R. F. Knacke, Y. J. Pendleton, *Icarus* **124**, 625 (1996).
43. K. Stamnes, S. Tsay, W. Wiscombe, K. Jayweera, *Appl. Opt.* **27**, 2502 (1988).
44. E. Lellouch *et al.*, *Icarus* **79**, 328 (1989).
45. R. V. Yelle, D. F. Strobell, E. Lellouch, D. Gautier, in *Huygens: Science Payload and Mission, Vol. ESA-SP 1177*, A. Wilson, Ed. (European Space Agency Publications Division, Noordwijk, Netherlands, 1997), pp. 243–256.
46. N. Husson, B. Bonnet, N. A. Scott, A. Chédin, *The "GEISA" data bank 1991 version* (Internal note L.M.D. 163, Laboratoire de Météorologie Dynamique, Palaiseau, France, 1991).
47. W. M. Grundy, B. Schmitt, E. Quirico, *Icarus* **155**, 486 (2002).
48. M. T. Lemmon, E. Karkoschka, M. Tomasko, *Icarus* **103**, 329 (1993).
49. C. A. Griffith, *Nature* **364**, 511 (1993).
50. T. B. McCord *et al.*, *J. Geophys. Res.* **103**, 8603 (1998).
51. T. B. McCord, personal communication.

52. We thank D. Cruikshank for helpful discussions regarding the spectroscopic characteristics of complex organic molecules. This research is supported by the NASA Planetary Astronomy Program.

24 December 2002; accepted 24 March 2003

Adaptation in a Plant-Hummingbird Association

Ethan J. Temeles[1]* and W. John Kress[2]

Sexual dimorphism in bill morphology and body size of the Caribbean purple-throated carib hummingbird is associated with a reversal in floral dimorphism of its *Heliconia* food plants. This hummingbird is the sole pollinator of *H. caribaea* and *H. bihai*, with flowers of the former corresponding to the short, straight bills of males, the larger sex, and flowers of the latter corresponding to the long, curved bills of females. On St. Lucia, *H. bihai* compensates for the rarity of *H. caribaea* by evolving a second color morph with flowers that match the bills of males, whereas on Dominica, *H. caribaea* evolves a second color morph with flowers that match the bills of females. The nectar rewards of all *Heliconia* morphs are consistent with each sex's choice of the morph that corresponds to its bill morphology and energy requirements, supporting the hypothesis that feeding preferences have driven their coadaptation.

Understanding natural adaptations of organisms to their environment has been the focus of evolutionary investigations since the time of Darwin (*1*) and Wallace (*2*). Plant-animal interactions, especially those between flowering plants and their animal pollinators, provide classic examples of hypothesized coadaptations that confer advantages to both mutualists (*3*, *4*). The most convincing investigations of adaptation require (i) the presence of discrete character polymorphisms in natural populations, (ii) evidence for the genetic basis of this variation, (iii) fitness measures, and (iv) comparative studies among populations (*5*). Here we present comparative data from two Lesser Antillean islands on contemporary character polymorphisms in sympatric species of the tropical plant genus *Heliconia* and their common pollinator, the purple-throated carib hummingbird, which support the principle of coadaptation between these mutualists.

The purple-throated carib hummingbird, *Eulampis jugularis*, is an example of sexual dimorphism that results from ecological causation: Although the wings and body masses of males average 8.6 and 25%, respectively, larger than those of females, the bills of females average 30% longer than those of males and are 100% more strongly curved (*6*, *7*). Temeles *et al.* (*7*) showed that *E. jugularis* is the sole pollinator of two species of *Heliconia* on St. Lucia, a green-bracted *H. bihai* whose long, curved flowers match the bills of females and a red-bracted *H. caribaea* whose short, straight flowers match the bills of males (Fig. 1, A to E and G). Each sex prefers and feeds most efficiently from the *Heliconia* species whose flowers correspond to its bill size and shape, which is consistent with the predictions of ecological causation and feeding adaptation (*7*). At forest reserves on St. Lucia where the red-bracted *H. caribaea* is absent or rare, a red-green–bracted morph of *H. bihai* takes its place and has shorter, straighter flowers with a morphology intermediate between those that correspond to the bill morphologies of males and females (Fig. 1F). Male *E. jugularis* at these sites are associated primarily with the red-green–bracted morph of *H. bihai*,

[1]Department of Biology, Amherst College, Amherst, MA 01002 USA. [2]Botany, MRC-166, United States National Herbarium, National Museum of Natural History, Post Office Box 37012, Smithsonian Institution, Washington, DC 20013–7012 USA.

*To whom correspondence should be addressed. E-mail: ejtemeles@amherst.edu